Added value of convection-permitting simulations for understanding future urban humidity extremes

Langendijk, Gaby S.; Rechid, Diana; Sieck, Kevin; Jacob, Daniela

Published in:
Weather and Climate Extremes

DOI:
10.1016/j.wace.2021.100367

Publication date:
2021

Document Version
Publisher's PDF, also known as Version of record

Weather and Climate Extremes 33 (2021) 100367

Contents lists available at ScienceDirect

Weather and Climate Extremes

journal homepage: www.elsevier.com/locate/wace

Added value of convection-permitting simulations for understanding future urban humidity extremes: case studies for Berlin and its surroundings

G.S. Langendijk [a,b,*], D. Rechid [a], K. Sieck [a], D. Jacob [a,b]

[a] Climate Service Center Germany (GERICS), Helmholtz-Zentrum Hereon, Fischertwiete 1, 20095 Hamburg, Germany
[b] Faculty of Sustainability, Leuphana University of Lüneburg, Universitätsallee 1, 21335 Lüneburg, Germany

ARTICLE INFO

Keywords:
Urban-rural contrasts
Humidity
Future climate extremes
Regional climate modelling
Convection permitting

ABSTRACT

Climate extremes affected cities and their populations during the last decades. Future climate projections indicate climate extremes will increasingly impact urban areas during the 21st century. Humidity related fluctuations and extremes directly underpin convective processes, as well as can influence human health conditions. Regional climate models are a powerful tool to understand regional-to-local climate change processes for cities and their surroundings. Convection-permitting regional climate models, operating on very high resolutions, indicate improved simulation of convective extremes, particularly on sub-daily timescales and in regions with complex terrain such as cities. This research aims to understand how crossing spatial resolutions from ~12.5 km to ~3 km grid size affect humidity extremes and related variables under future climate change for urban areas and its surroundings. Taking Berlin and its surroundings as the case study area, the research identifies two categories of unprecedented future extreme atmospheric humidity conditions happening under 1.5 °C and 2.0 °C mean warming based on statistical distributions, respectively near surface specific humidity >0.02 kg/kg and near surface relative humidity <30%. Two example cases for each future extreme condition are dynamically downscaled for a two months period from the 0.44° horizontal resolution following a double-nesting approach: first to the 0.11° (~12.5 km) horizontal resolution with the regional climate model REMO and thereafter to the 0.0275° (~3 km) horizontal resolution with the non-hydrostatic version of REMO. The findings show that crossing spatial resolutions from ~12.5 km to ~3 km grid size affects humidity extremes and related variables under climate change. Generally, a stronger decrease in moisture (up to 0.0007–0.005 kg/kg SH and 10–20% RH) and an increase in temperature (1–2 °C) is found on the 0.0275° compared to the 0.11° horizontal resolution, which is more profound in Berlin than in the surroundings. The convection-permitting scale mitigates the specific humidity moist extreme and intensifies the relative humidity dry extreme in Berlin, posing challenges with respect to health for urban dwellers.

1. Introduction

Urban populations have become increasingly affected by climate extremes over the course of the last decades (Masson et al., 2020; Mishra et al., 2015; Rosenzweig et al., 2018). Climate projections indicate extreme events will further increase in frequency and intensity in the future under climate change (Alexander, 2016; IPCC et al., 2012; Myhre et al., 2019). Urban areas and its population are prone to the impacts of climate extremes, for instance heatwaves and heavy precipitation (Grimmond et al., 2010; Rosenzweig et al., 2018). Commonly investigated underlying climatic variables, such as temperature and mean precipitation are relatively well understood for urban areas (Argüeso et al., 2016; Wiesner et al., 2018). Other climatic variables such as humidity and particularly its extremes, are less commonly investigated despite their critical importance to urban areas.

Humidity fluctuations and extremes are key to convective meteorological phenomena and related extreme events. It is a direct source of water influencing the intensity and frequency of precipitation events, droughts, as well as heatwaves (Fischer and Knutti, 2013; Hardwick Jones et al., 2010). High humidity levels combined with high temperatures result in greater thermal stress for humans, and can lead to increased mortality rates, especially during heat waves (Coccolo et al., 2016; Raymond et al., 2020). Exposure to heat-humidity extremes is projected to increasingly pose health challenges to the global population

* Corresponding author. Climate Service Center Germany (GERICS), Helmholtz-Zentrum Hereon, Fischertwiete 1, 20095 Hamburg, Germany.
E-mail address: gaby.langendijk@hereon.de (G.S. Langendijk).

https://doi.org/10.1016/j.wace.2021.100367
Received 15 February 2021; Received in revised form 28 May 2021; Accepted 5 August 2021
Available online 8 August 2021

in the upcoming decades under 1.5° and 2.0 °C warming (Li et al., 2020). Whereas, low humidity levels can lead to more severe influenza epidemics by providing the right conditions for influenza spread and survival, particularly in fall and winter in temperate climates (Dalziel et al., 2018; Davis et al., 2016; Lowen et al., 2007; Shaman and Kohn, 2009). Much of the observed wintertime increase of mortality in temperate regions is attributed to influenza (Shaman et al., 2010). This shows that humidity levels can impact human health. It is therefore pivotal to understand humidity fluctuations and extremes, particularly under future climate change.

To gain a thorough understanding on humidity extremes and their impacts it is critical to advance the knowledge on the drivers of humidity extremes, at various spatial scales, and particularly in a multivariate context with a focus on process understanding (Bai et al., 2018; Fischer and Knutti, 2013; Sharma et al., 2013; Sillmann et al., 2017). Improved regional-to-local understanding of humidity extremes under climate change for cities supports the development of climate information tailored to the needs of urban decision-makers and stakeholders, to inform adaptation towards increased resilience in urban areas (Aerts and Botzen, 2014; Bai et al., 2018; Baklanov et al., 2018; Langendijk et al., 2019a). Regional climate models (RCMs) are a powerful tool to understand meteorological processes on regional-to-local scales under climate change, as they simulate multivariate dynamical interactions including those of urban areas and their surroundings. RCMs currently simulate a variety of horizontal grid resolutions, from roughly 50 km × 50 km, to 12.5 km × 12.5 km, and further down to 3 km × 3 km grid resolutions (Jacob et al., 2020). The very high horizontal resolution of 3 km × 3 km, the so-called convection-permitting scale, offers promising prospects to improve the simulation of convective systems, clouds, and precipitation, particularly for areas with complex terrain such as cities (Ban et al., 2014; Coppola et al., 2020; Masson et al., 2020; Prein et al., 2015). Previous studies indicate convection-permitting simulations particularly show large benefits on sub-daily timescales and for extreme values, compared to little improvements for mean values averaged over time (Argüeso et al., 2016; Prein et al., 2015). Despite being propitious, until now, no research investigated whether or not finer spatial resolutions improve the understanding and simulation of future humidity extremes for cities.

Two main humidity variables are investigated in this research. Firstly, specific humidity, which is the amount of water vapor in relation to the total mass of water vapor and air combined, expressed in kilograms of water vapor per kilogram of moist air. Secondly, relative humidity, which indicates how saturated the air is compared to the water vapor fully saturated air could contain at a specific temperature, expressed as a percentage. The following abbreviation are used in this research for referring to specific humidity: SH, and relative humidity: RH.

This study takes Berlin and its surroundings as the case study area. Prior research shows urban areas are generally less moist than its surroundings, often referred to as the urban dry island (UDI) effect (Hage, 1975; Langendijk et al., 2019b; Lokoshchenko, 2017). Langendijk et al. (2019b) indicates that Berlin shows an increase in specific humidity, and a decrease in relative humidity until the end of the century. The latter is stronger in Berlin than in its surroundings. It remains unknown how urban areas, for instance through this "drying" effect, influence the meteorological conditions characterizing humidity extremes.

By the authors' knowledge, there has been no study until now that investigates if increased model resolutions affects the simulation of urban-rural meteorological processes for unprecedented future humidity extremes under climate change. Therefore, with a focus on Berlin, this first study is centered on the following research question: "How does crossing spatial resolutions from ~12.5 km to ~3 km grid size affect unprecedented future humidity extremes and related variables under climate change for Berlin and its surroundings?"

2. Method

The research contains three main methodological parts: 1) the identification of unprecedented future extreme conditions for the Berlin region; 2) new experiment set up for downscaling extremes; 3) analysis of the downscaled model output data.

2.1. Research area

Berlin and its surroundings are selected as the case-study region, because of the relatively flat regional topography, Berlin's large city size, and the distinct urban-rural landscape heterogeneity. These aspects make Berlin and its surroundings suitable to investigate urban-rural contrasts using regional climate model output data.

Berlin, the capital of Germany, is a large-scale city with around 3.6 million inhabitants covering approximately 891.1 km^2 (Amt für Statistik Berlin-Brandenburg, 2020), located in-land at approximately 52.52° N, 13.4° E. The land cover of Berlin's surroundings is roughly 50% agricultural and grass land, 36% forest and 14% build up areas and water bodies (Fig. 1b) (Amt für Statistik Berlin-Brandenburg, 2020). The primary investigated domain is approximately 140 km by 140 km centered around Berlin (black rectangular, Fig. 1b).

2.2. Identifying future extreme conditions

2.2.1. Models and data

The first step of the research identifies future extreme conditions related to atmospheric moisture, occurring under 1.5 °C and 2.0 °C global warming. This research uses the model output data produced by the "Half a degree Additional warming, Prognosis and Projected Impacts" (HAPPI) project (Mitchell et al., 2017; Sieck et al., 2021). This dataset is a unique modelling effort that aims at generating large ensembles of climate model simulations which enable investigations on how the climate, and in particular extreme events, might differ from present day under 1.5 °C and 2.0 °C warmer futures than pre-industrial conditions. The HAPPI global circulation model (GCM) simulations use prescribed sea-surface temperatures (SST) for respective periods, following the Atmospheric Model Intercomparison Project (AMIP) style (Gates, 1992). Three simulation periods are selected: a historical decade (2006–2015) with observed SSTs, and two projected periods with 1.5 °C and 2.0 °C warmer global mean surface temperature than pre-industrial (1861–1880) conditions. For the latter two periods, CMIP5 mean SST anomaly patterns for the respective global warming are added to the observed SST pattern used for the historical decade. Lastly, greenhouse gas forcing is constructed from RCP2.6 and RCP4.5 emission scenarios, respectively. For each period a large ensemble of simulations are performed, each member initialized with slightly different initial conditions, leading to a large ensemble of possible climates. A detailed description of the HAPPI experiment design can be found in Mitchell et al. (2017).

From the larger HAPPI consortium, the ensemble simulations from the GCMs are dynamically downscaled by the regional climate model REMO (Sieck et al., 2021). The REMO 2015-HAPPI version (Jacob et al., 2012a) was applied for the standard European CORDEX domain on a 0.44° (~50 km) horizontal resolution, using the boundary conditions from the HAPPI GCM model ECHAM6 (Stevens et al., 2013) with 100 members per period, resulting in a total of 1000 model output years for each global warming period (3000 years of climate data). The large number of model output years can cover a wide range of possible extremes, leading to more robust statistics and results. The HAPPI model output data is available on a daily resolution. A further description of the downscaling approach can be found in Sieck et al. (2021).

2.2.2. Extreme event distributions

Statistical distributions of the historical, 1.5 °C, and 2.0 °C periods are calculated from the HAPPI data to identify future extreme conditions

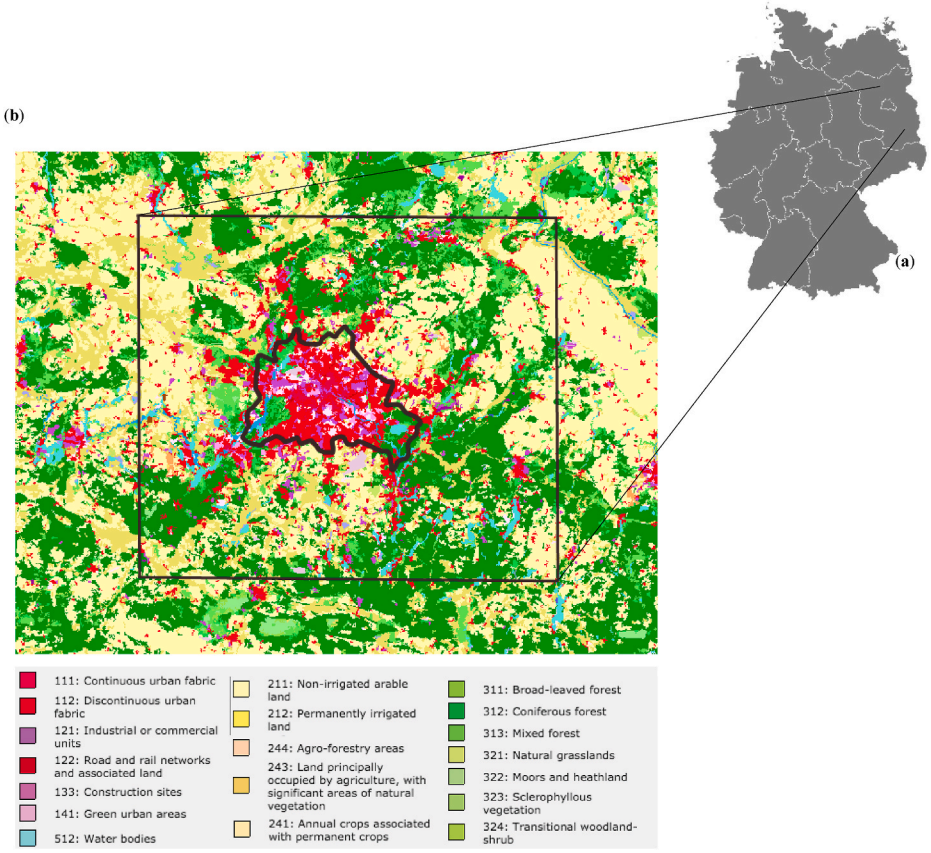

Fig. 1. Research area. (**a**) Germany and (**b**) a land-cover map indicating Berlin's administrative boundaries (black polygon) and research domain including the surroundings (black rectangular). Land cover following CORINE land cover map (EEA, 2000; Langendijk et al., 2019b).

under 1.5 °C and 2.0 °C global mean warming, particularly related to moisture.

A domain centered around Berlin is selected, consisting of four grid boxes (Annex Fig. A1) that approximately match the primary domain of investigation showed in Fig. 1. The studied variables are: specific humidity (SH), relative humidity (RH), 2m-temperature, 2m-minimum temperature, 2m-maximum temperature and precipitation. Two types of extreme value distributions are calculated in order to define categories of unprecedented future extreme events under and/or above a specific humidity threshold. Firstly, the generalized extreme value probability density function (GEV-PDF) over the 90th and 10th percentile of each variable is computed for each period over the spatially averaged domain (Annex Fig. A1). The GEV-PDF constructs a distribution over the values above the 90th and below the 10th percentile for all years for each variable. For RH and SH the 5th and 95th percentile distributions are also calculated. Secondly, the GEV-PDF is calculated over the block maxima and block minima of each variable for each year for all ensemble members in each period. The block maxima and minima are respectively the largest and smallest values within each simulated year. Based on the tails of the distributions the extreme conditions are selected that only happen under 1.5–2.0 °C mean warming and do not occur during the historical period.

2.3. Downscaling

2.3.1. Models

The identified extreme conditions based on the HAPPI (0.44°) model output data (ECHAM6 -REMO2015) are downscaled following a double-nesting approach with a first downscaling step to the 0.11° horizontal resolution (~12.5 × 12.5 km grid box size) by REMO (2015-HAPPI version) and thereafter to the 0.0275° horizontal resolution (~3 × 3 km grid box size) by applying the non-hydrostatic, convection-permitting version of REMO (REMO-NH, 2015-HAPPI version).

The regional climate model REMO is a three-dimensional, hydrostatic limited-area model of the atmosphere that has been extensively used and tested in climate change studies for Europe (Jacob et al., 2012b; Kotlarski et al., 2014). It originates from the 'Europa-Modell' of the German Weather Service (DWD) (Majewski, 1991). The physical parameterizations are largely based on the global climate model ECHAM-4 (Roeckner et al., 1996) and have been further developed over the course of the last decades. Model specifications can be found in Jacob et al. (2012a) and in Jacob and Podzun (1997).

The land cover scheme within REMO follows a tile approach, based on three basic land surface types; land, water, and sea ice. Subgrid fractions are specifying further land cover types, including an urban sub-fraction. These fractions are not assumed to be located in a specific area of a grid box, but cover a percentage of the total grid box area, together summing up to 100 %. The turbulent surface fluxes and the surface radiation flux are calculated separately for each tile and are subsequently averaged within the lowest atmospheric level using the respective areas as weights (Rechid and Jacob, 2006; Semmler, 2002).

For the urban sub-fraction, the REMO model follows the so-called 'bulk'-approach. Sealed urban areas are represented as a rock surface, which is described in the model by a relatively high roughness length, high albedo, and no water storage capacities (Langendijk et al., 2019b). Langendijk et al. (2019b) indicates that the simple urban bulk-scheme shows the urban-rural contrast for temperature and humidity variables. The simple scheme is less skilled in simulating the timing of the peak of the urban heat island at night.

The hydrostatic approximation used in climate models fails for grid sizes smaller than 10 × 10 km (Prein et al., 2015) making the RCM's solution less reliable at those spatial resolutions. Therefore the

non-hydrostatic model version REMO-NH was developed to directly resolve the vertical momentum equation, leading to a better representation of small-scale mesoscale circulations and convection (Goettel, 2009). In addition, REMO-NH more accurately represents the surface and orography fields. The non-hydrostatic formulation significantly improves model simulation output on fine horizontal resolutions, particularly for mountainous regions and urban areas (Argüeso et al., 2016; Ban et al., 2014; Coppola et al., 2020; Prein et al., 2015).

2.3.2. Set-up

A downscaling experiment set-up is developed to downscale the identified extreme conditions from the 0.44° spatial scale to finer spatial and temporal resolutions, particularly tailored to the needs of this research.

The domain sizes are defined for the 0.11° and 0.0275° horizontal resolutions to support the double-nesting approach. Matte et al. (2017) show that the distance needed for the small-scale features (so-called spatial spin-up) to develop is proportional to the jump of resolution (Matte et al., 2016). The boundaries used within our nesting approach (e.g. the boundaries of the nested model and our analysis domain) is respecting the spatial spin-up zone as recommended by Matte et al. (2017). The resulting domains for the double-nesting downscaling are presented in Fig. 2. The domains have a size of respectively 129 × 129 grid boxes centered around Berlin for the 0.11°, as well as for the 0.0275° horizontal resolution. The domains are selected based on the above rationale, whilst balancing computing costs and the strength of the boundary forcing in order for the model to capture the extreme when downscaled.

The appropriate spin-up time is determined to be around 15 days. This is comparable to spin-up times set by similar studies (Leps et al., 2019; Matte et al, 2016, 2017). The spin-up time is tested for REMO (0.11°) and REMO-NH (0.0275°) for one case of each identified extreme. The following model output variables are investigated: SH, RH, 2m-temperature, evaporation, soil wetness, soil temperature, deep soil temperature, surface pressure, vertically integrated SH, and surface sensible heat flux. A stable state is found for most variables within 1–4 days after starting the simulation, and after ~10 days for 2m-temperature, surface pressure, evaporation, soil wetness (not shown). This is in line with studies by Denis et al. (2002) and Jerez et al. (2020). Following similar studies, the total simulation period for downscaling each extreme condition is 2 months for the first downscaling step from 0.44° to 0.11° horizontal resolution, and 1.5 month for the second step from 0.11° to 0.0275° horizontal resolution (Denis et al., 2002; Herceg et al., 2006; Leps et al., 2019; Matte et al, 2016, 2017). The nesting interval frequency for downscaling the HAPPI data to the 0.11° horizontal resolutions is 6-hourly, and 1-hourly for further downscaling from the 0.11° to the 0.0275° horizontal resolution. The time step for all downscaled simulations is 60 seconds. The downscaled model output data is available on an hourly temporal resolution.

2.4. Data analysis

The analysis of the model output data across the spatial resolutions (0.11°, 0.0275°) is focused on Berlin and its direct surroundings (Fig. 1b). In order to compare the results across the horizontal scales, a coherent masking approach is developed to distinguishing Berlin from its surroundings. The urban area is defined by the grid cells containing an urban fraction larger than 0.3 as prescribed by the REMO land surface cover scheme. The grid boxes with an urban fraction >0.3 outside of the administrative boundaries of Berlin are excluded from the city mask (black polygon, Fig. 1b). This approach is followed for both horizontal resolutions. The resulting city masks for 0.11° and 0.0275° horizontal resolutions cover relatively similar areas for Berlin, with the 0.0275° mask capturing the actual city size and boundaries more accurately (Fig. 3). The masks for the surroundings include all grid boxes outside the city mask and within the primary domain of interest of 140 km by 140 km centered around Berlin (black rectangular, Fig. 1b). Table 1 shows the amount of grid boxes for different urban fractions for Berlin on the 0.11° and 0.0275° horizontal resolutions.

The downscaled extreme conditions are studied with a focus on understanding meteorological processes characterizing the extreme conditions. The following 14 model output variables are spatially averaged over the grid boxes representing Berlin (black polygon Fig. 1) and its surroundings (black rectangle Fig. 1) and thereafter analyzed: SH, RH, 2m-temperature, 2m-maximum temperature, 2m-minimum temperature, surface evaporation, relative soil moisture, soil temperature, surface pressure, 10-m wind speed, vertically integrated SH (integrated over the total atmospheric column up to the model top), surface sensible heat flux, sensible latent heat flux, and total precipitation. The analysis particularly focusses on four aspects: 1) differences due to spatial resolution (0.11° vs. 0.0275°); 2) urban-rural contrast (Berlin vs. surroundings); 3) comparison of cases (two examples of each selected extreme condition); 4) cross-comparing selected extreme conditions.

One additional analysis is performed to understand if the models on the different horizontal resolutions (0.11° and 0.0275°) behave similarly to the observations and in order to put the results for the humidity extremes into context. Observations are compared with historical model output data for the months when the selected extremes occur, for the time slice 1996–2005. The hourly in-situ measurements are obtained from the DWD Climate Data Center (DWD, 2019), stemming from ten observation stations, of which six are located in Berlin, and four in the surroundings of Berlin. The observation stations and their respective locations are presented in the appendix of Langendijk et al. (2019b). DWD does not provide in-situ observations for specific humidity. Therefore, specific humidity is derived from observed mean daily vapor pressure (e) in hPa and air pressure (P) in hPa from observations (DWD, 2021), using the following formula (Stull, 2017):

$$Specific\ humidity = \frac{\varepsilon * e}{P - e*(1 - \varepsilon)} \quad (1)$$

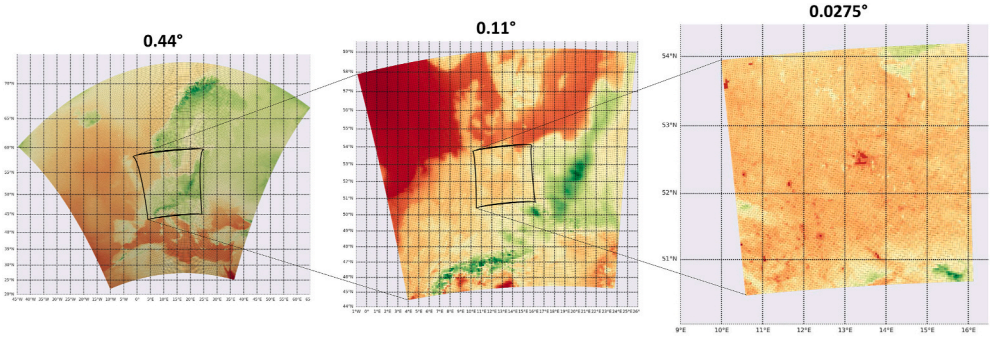

Fig. 2. The domains for the double-nesting approach, the HAPPI (0.44°) standard European domain (left), the 0.11°-domain (middle) and the 0.0275°-domain (right).

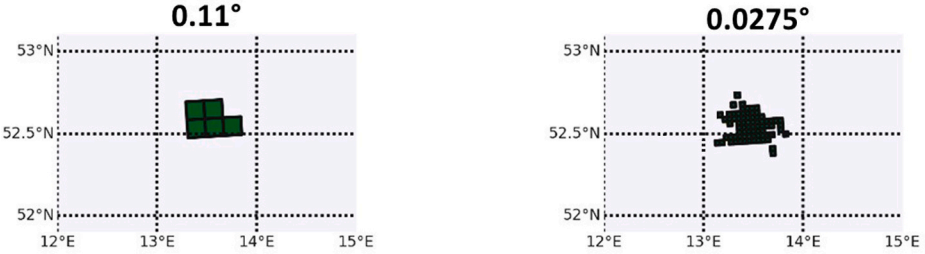

Fig. 3. Masks for Berlin, based on urban fraction > 0.3 for 0.11° (left) and 0.0275° (right) horizontal resolutions.

Table 1
Amount of grid boxes for different urban fractions for Berlin on the 0.11° and 0.0275° horizontal resolutions.

	Amount of grid boxes	
Urban fraction	0.11°	0.0275°
>0.3	5	76
>0.4	3	63
>0.5	3	60
>0.6	2	47
>0.7	2	42
>0.8	0	30
>0.9	0	20
1	0	18

Where $\varepsilon = 0.622$ g vapor/g dry air is the ratio of gas constants for dry air to that for water vapor.

The model data consists out of EURO-CORDEX REMO2015 transient model simulations on a 0.11° horizontal resolution driven by the MPI-ECHAM6 model, and the REMO-NH (version 2015, driven by REMO 2015) model output data on convection-permitting scales produced as a part of the European Climate Prediction system project (EUCP) for the period 1996–2005 (Lowe et al., 2020). The main variables of interest are investigated, respectively RH, SH and temperature, to understand the general differences between the horizontal resolutions and observations.

3. Results

The result section is divided into two main parts: 1) identification of unprecedented future extreme conditions and respective meteorological process understanding; 2) analysis of the downscaled extreme conditions across spatial and temporal scales. The discussion of the results is directly carried out while presenting the findings throughout the results section.

3.1. Future extreme conditions

3.1.1. Identification of future extreme conditions

Statistical distributions are calculated based on the HAPPI data (0.44°, ECHAM6-REMO2015) to identify future extreme conditions (see section 2.2.2). Generally, the investigated domain shows a shifted mean with warmer (~1–2 °C) and more humid (SH) conditions under 1.5 °C and 2.0 °C, which is more profound under 2.0 °C (Annex, Fig. A2). The 90th and 95th percentile distributions for relative humidity show a decrease in RH for 1.5 °C and 2.0 °C compared to historical simulations, and an increase in RH for the 5th and 10th percentile distributions. The RH block maxima and minima distributions both show a slight decrease in moisture for 1.5 °C and 2.0 °C warming compared to the historical decade, particularly for the block minima. The percentile distributions for precipitation do not show a clear tendency. The precipitation block maxima shows increased frequency and intensity of rain extremes, particularly under 2.0 °C warming (Annex, Fig. A2).

Generally, there is an increase in the intensity and frequency visible for the tail-extremes under 1.5 °C and 2.0 °C warming compared to the historical decade, for the block maxima distributions for 2m-temperature, 2m-minimum temperature, 2m-maximum temperature, precipitation, SH, and for the block minima distributions for RH. These tail-extremes are more profound under 2.0 °C warming than 1.5 °C warming (Annex, Fig. A2).

This research particularly concerns moisture related variables, respectively SH and RH. Based on the above findings, the block maxima for SH and block minima for RH are therefore further investigated to identify future extreme conditions. Fig. 4 shows the respective distributions for SH (block maxima) and RH (block minima). In the tails of both distributions, roughly above 0.02 kg/kg SH and below 30 % RH, extreme conditions occur that only happen under 1.5 °C and 2.0 °C warming, and not during the historical decade. The thresholds SH>0.02 kg/kg and RH<30 % are therefore selected to further investigate extreme conditions.

The selected thresholds, SH>0.02 kg/kg and RH<30 %, occur 0 days in the historical decade simulated by the HAPPI ensemble members. For SH>0.02 kg/kg, the threshold is surpassed 2 days under 1.5 °C warming, and 10 days under 2.0 °C warming. For RH<30 %, the threshold is surpassed 6 days under 1.5 °C warming, and 5 days under 2.0 °C warming. These extreme condition days occur in different years of the simulated decades and within different ensemble members of the HAPPI dataset. In-situ observations for relative humidity daily means (DWD, 2019) show that, although extreme conditions of around 30–40% exists, no extreme conditions of RH<30 % occurred in Berlin and its surroundings during the respective simulated historical period (2006–2015). The specific humidity values derived from the DWD in-situ observations for 2006–2015 do not show values larger than 0.02 kg/kg. This indicates that the selected extreme conditions, SH>0.02 kg/kg and RH<30 %, are a category of unprecedented future extreme humidity events.

3.1.2. Meteorological process understanding of future extreme conditions

The main meteorological characteristics are investigated for the extreme condition days surpassing the SH>0.02 kg/kg and RH<30 % thresholds, in order to understand whether the extreme conditions show similarities and to identify representative extreme conditions for further downscaling. This analysis also verifies if the extreme conditions are an artifact of one ensemble member, or a result of odd, not physically plausible, model behavior.

The findings show that all extreme condition SH>0.02 kg/kg days occur in July and August, and are characterized by very high specific humidity values (SH: 0.020–0.023 kg/kg), mean daily temperature of around 30 °C, and maximum daily values reaching almost 40 °C shortly before and during the peak of the extreme condition. Generally, warm air can hold more moisture than cold air, therefore the high specific humidity levels are expected to occur during these warm summer days. No precipitation occurs during the extreme condition and the incoming shortwave radiation is relatively high (250 W/m^2) compared to the mean of the historic decade (100 W/m^2) (Table 2). During the weeks before the extreme condition precipitation occurs within regular bounds, providing the soil with sufficient moisture content (soil moisture >0.7). This enables relatively high latent heat fluxes and therefore

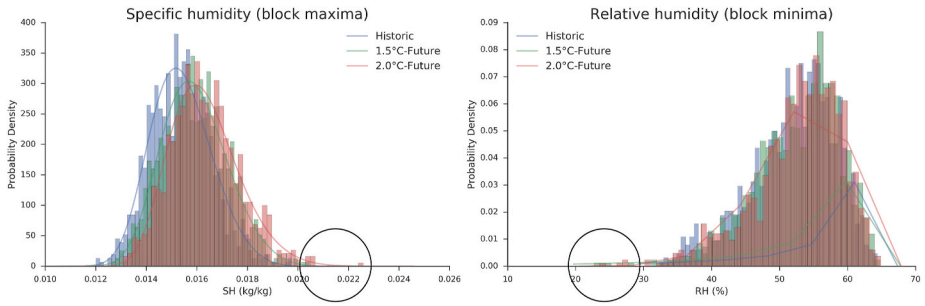

Fig. 4. The block maxima for SH (left) and block minima for RH (right) distributions based on the HAPPI ensemble members for the historical decade (1996–2005), 1.5 °C and 2.0 °C simulated periods.

Table 2
Daily mean values calculated over all ensemble members of each extreme condition for 1.5 °C and 2.0 °C future warming, compared to the overall mean of the historical decade (1996–2005).

	SH>0.02 kg/kg		RH<30 %	
Variables	*1.5°C*	*2.0°C*	*1.5°C*	*2.0°C*
SH (kg/kg)	0.02015	0.0211	0.0019	0.0017
RH (%)	79	74	27	26.25
2m-temperature (°C)	29.4	30.4	8.5	9
2m-maximum temperature (°C)	36	37	11.3	13
2m-minimum temperature (°C)	23.5	24.5	7	6.5
Soil wetness (m)	0.37	0.38	0.34	0.22
Relative soil moisture (%)	0.86	0.88	0.79	0.51
Surface pressure (Pa)	101700	101400	101060	102000
Shortwave radiation (W/m2)	259	261	44	66
Longwave radiation (W/m2)	425	433	277	271
Sensible heat flux (W/m2)	5	10	−35	−38
Latent heat flux (W/m2)	143	65	12	7
Precipitation (kg/m2/s)	0.00001	0.000019	~0	~0
Surface wind speed (m/s)	2.6	2.6	6.7	6.7

high evaporation rates shortly before and during the extreme condition (Table 2). These meteorological conditions are driven by the synoptic weather conditions of a warm front, where temperatures and moisture rise after the warm front replaced the cold air mass. Before the warm front passes precipitation is likely to occur, and after the warm front the skies become clear, and temperatures as well as humidity levels increase. This is the so-called warm sector. The combination of the above meteorological characteristics lead to extreme days with SH>0.02 kg/kg. A visualization describing the meteorological processes is provided in Fig. 5. In addition, Table 2 shows the mean values of all extreme conditions for each variable, as well as the comparison to the respective overall mean values of the historical decade.

All extreme condition RH<30 % days occur in November, and are characterized by very low relative humidity (RH: 23–30 %) and specific humidity (SH: 0.0016–0.0020 kg/kg) values (Table 2). During the autumn months before the extreme condition occurs, the relative soil moisture is lower than usual for most (approx. 80 %) ensemble members (not shown). In the course of the days before the extreme only little precipitation occurs. The mean daily temperature is around 9 °C. The incoming shortwave radiation is lower than the historical average, as well as the relative soil moisture and latent heat flux (Table 2). The meteorological characteristics indicate that this extreme is driven by the synoptic weather condition of a passing cold front. The high wind speeds (~6.7 m/s) are also typical for a fast moving cold front (Fig. 5, Table 2). After the cold front passes the skies clear up, surface pressure increases, and the dry air advection leads to low humidity levels (Spänkuch et al., 2011). The combination of the above meteorological characteristics lead to the extreme days with RH<30 %. A visualization describing the meteorological processes is provided in Fig. 5.

All the extreme days of each individual extreme condition, SH>0.02 kg/kg and RH<30 %, show similar meteorological characteristics. This similarity among the extreme days implies that the identified extreme conditions (SH>0.02 kg/kg and RH<30 %) are not physically improbable model artifacts.

The extreme condition days are generally slightly extremer under 2.0 °C than under 1.5 °C warming, up to 0.03 kg/kg moister (SH) and 3 % less moist (RH). Particularly for SH>0.02 kg/kg the extreme days occur more frequent under 2.0 °C warming, respectively 10 days compared to 2 days under 1.5 °C warming. Warm air can hold more moisture than cold air, therefore it can be expected that higher global mean global temperatures could lead to more extreme moist days, particularly in summer. In total 4 ensemble members, 2 ensemble members each for both RH<30 % and SH>0.02 kg/kg, show two consecutive days of the extreme condition under 2.0 °C warming. No consecutive extreme days occur under 1.5 °C. This indicates humidity extremes might occur more frequent and could last longer under 2.0 °C warming compared to 1.5 °C warming, and could potentially become even more profound under stronger temperature increase. This is in line with previous studies, such as Alexander (2016) and IPCC et al. (2012). For each threshold (SH>0.02 kg/kg and RH<30 %) two ensemble member extreme condition examples, further referred to as cases, are selected for further downscaling. The cases are picked from the simulated decades with a 2.0 °C warmer future in order to understand the more extreme possible future conditions for Berlin and its surroundings. For both extreme conditions, SH>0.02 kg/kg and RH<30 %, the first example case (Case1) is a single day peak extreme condition and the

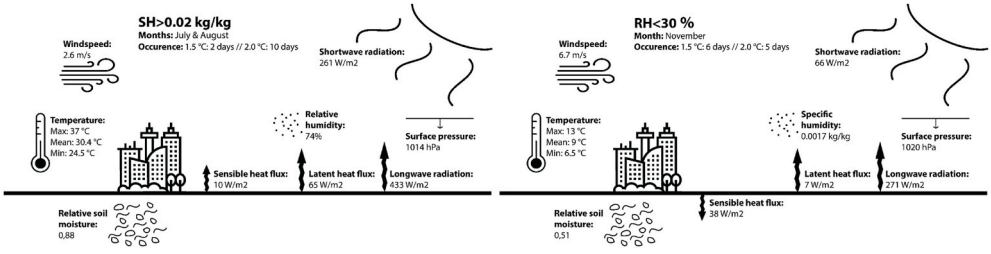

Fig. 5. Schematic visualization of meteorological characteristics of the extreme conditions SH>0.02 kg/kg (left) and RH<30 % (right), mean values for 2.0°C warming (see Table 2).

second example case (Case2) is an extreme condition lasting two consecutive days. The meteorological differences between the example cases of each extreme conditions are relatively similar. Therefore the final example cases for downscaling are arbitrarily selected from the available cases based upon the above criteria. The cases are labelled according to their extreme, respectively for SH>0.02 kg/kg CaseSH1 and CaseSH2, and for RH<30 % CaseRH1 and CaseRH2.

The example cases for each extreme condition can be described as follows. CaseSH1, with a peak value of 0.021 kg/kg SH, occurs in HAPPI ensemble member number 32 on 14 July in year 9 within the simulated decade under 2.0 °C warming. With a peak value of 0.023 kg/kg SH, CaseSH2 is simulated by HAPPI ensemble member number 87 and happens on 7 and 8 August in year 7. For RH<30 % CaseRH1, with a bottom low of 27 % RH, originates from HAPPI ensemble member number 26 and occurs on 10 November of year 2 of the simulated decade under 2.0 °C warming. With its lowest value of 25 % RH, CaseRH2 happens on 1 and 2 November in year 4 within the simulation of HAPPI ensemble member number 6.

3.2. Extremes across scales

3.2.1. Downscaled extreme conditions

Following the described double nesting approach (section 2.2.), Case1 and Case2 of each extreme condition, respectively SH>0.02 kg/kg and RH<30 %, are dynamically downscaled from 0.44° to 0.11°, and thereafter from the 0.11° to the 0.0275° horizontal resolution (Fig. 2).

A 1.5 month time series for all four downscaled cases, CaseSH1, CaseSH2, CaseRH1, and CaseRH2, is presented in Fig. 6 (SH>0.02 kg/kg, top row; RH<30 %, bottom row). The model output data shows that all four cases occur approximately around the same dates as in the original HAPPI data (0.44°), on the 0.11° as well as on the 0.0275° horizontal resolution. The extreme cases are clearly detectable for Berlin and its surroundings. CaseSH1 and CaseRH1 do not surpass the extreme conditions thresholds anymore, respectively SH>0.02 kg/kg and RH<30 %. Nevertheless an extreme peak is still clearly visible for these downscaled cases, almost reaching the respective extreme conditions thresholds. CaseSH2 and CaseRH2 do surpass the respective extreme conditions thresholds. This can be explained by the fact that Cases1 only just surpasses the extreme thresholds in the HAPPI data (by 0.001 kg/kg for CaseSH1 and 3 % for CaseRH1), and both Cases2 are two consecutive days in the HAPPI data and therefore result in more profound extreme values when downscaled to finer resolutions. In addition, the selected domain for downscaling has been relatively small with a strong boundary forcing, which enables the extreme condition to persist across model grid resolutions.

CaseSH1 and CaseSH2 of the SH>0.02 kg/kg extreme condition are surpassing the threshold of SH>0.02 kg/kg on additional dates besides the expected extreme event date in the downscaled simulation period, for the 0.11° and thereafter the 0.0275° horizontal resolution (Fig. 6). These extreme conditions are not present in the HAPPI (0.44°) data (not shown). These additional extreme conditions are on 19 July and around 30 July for CaseSH1, particularly surpassing the SH>0.02 kg/kg threshold around 30 July. A less distinct extreme condition can be found for CaseSH2 on 14 August, with a peak SH value of almost 0.2 kg/kg (Fig. 6). CaseRH1 and CaseRH2 of the RH<30 % extreme condition are spread over approximately 3–4 days on the 0.11° and 0.0275° horizontal resolution, compared to 1 day (Case1) and 2 days (Case2) at the 0.44° horizontal resolution.

The additional occurrence of the extremes for SH>0.02 kg/kg and the prolonged duration of the extremes for RH<30 % can be explained as follows. The coarser resolution (0.44°) averages values within a grid box over a relatively large area, as well as averages over the temporal resolution of a day mean. The land-atmosphere interactions and its fluxes get better resolved when the grid resolution increases to the 0.11° and thereafter the 0.0275° horizontal resolution. The finer grid boxes can generate larger and more peak values, resulting in additional extremes. Following similar rationale for the temporal scales, resolving fine temporal resolutions of up to an hour can prolong the duration of the extreme condition. This corresponds with similar findings for low-level aerosol concentration peaks in REMO by Pietikäinen et al. (2012).

Spatial maps are presented in Fig. 7 showcasing CaseSH1 and CaseRH1 during the peak hour of the extreme condition. The city boundaries and inner city differences are increasingly visible for Berlin on the 0.0275° horizontal resolutions for CaseSH1, showing a clear urban dry island. CaseRH1 shows Berlin moister than its surroundings on the 0.11° and hardly any urban-rural contrast on the 0.0275°

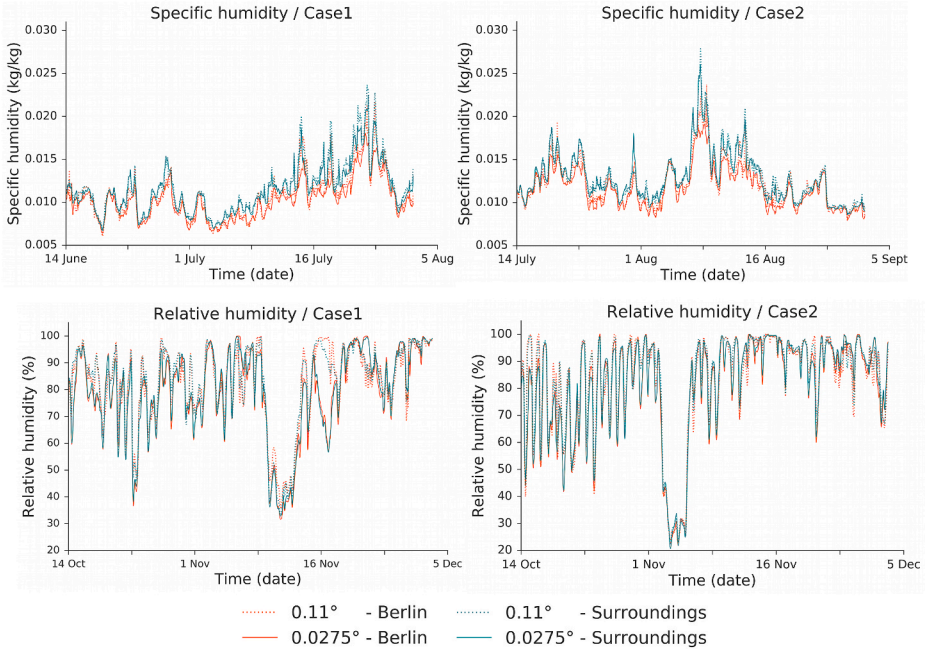

Fig. 6. The 1.5 month time series for Case1 and Case2 of both extreme conditions (SH>0.02 kg/kg, upper row; RH<30 %, bottom row) on 0.11° and 0.0275° horizontal resolutions, for Berlin and its surroundings.

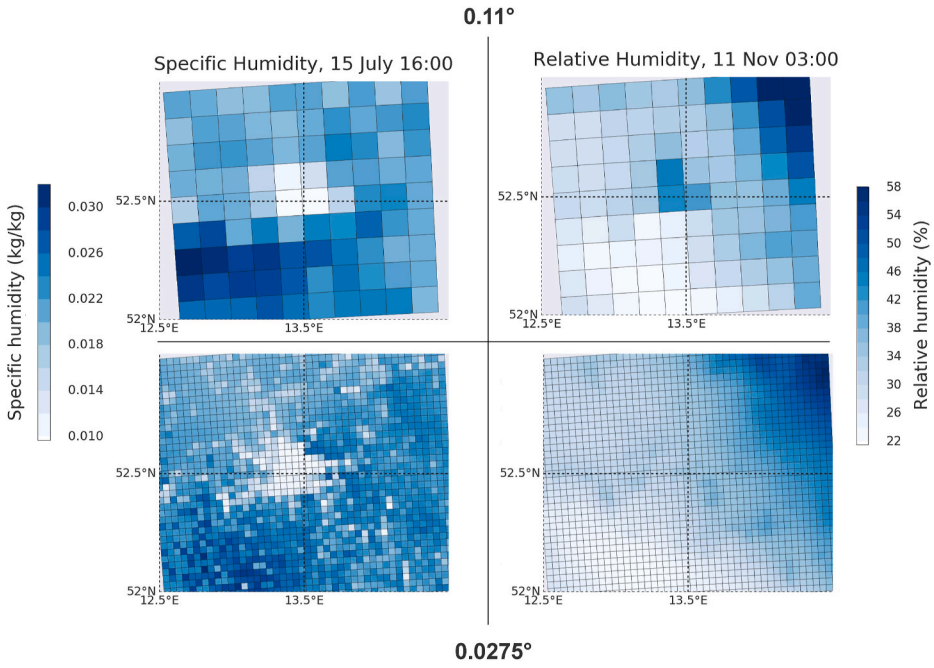

Fig. 7. Spatial maps for Berlin and its surroundings on the 0.11° (top row) and 0.0275° (bottom row) horizontal resolutions for SH for the peak hour of CaseSH1 (left column), and for RH for the peak hour of CaseRH1 (right column).

horizontal resolution. The reason behind the latter finding is further explained in section 3.2.3.

3.2.2. *Context of the extremes*

Before further analyzing the downscaled extreme conditions in more detail, the following analysis is presented to provide supporting context to interpret the results. Historical model output data from the EUCP dataset is compared with in-situ observations (DWD, 2021, 2019), for Berlin and its surroundings, on the 0.11° and 0.0275° horizontal resolution. Fig. 8 shows boxplots for the variables RH, SH, and temperature for the period 1996–2005, averaged over the months in which the extreme conditions occur, respectively July and August (SH>0.02 kg/kg), and October and November (RH<30 %).

The boxplots show that overall the models (0.11° and 0.0275°) are in line with the observations. Relative humidity is lower in Berlin than its surroundings for the observations and model data, by approximately 5

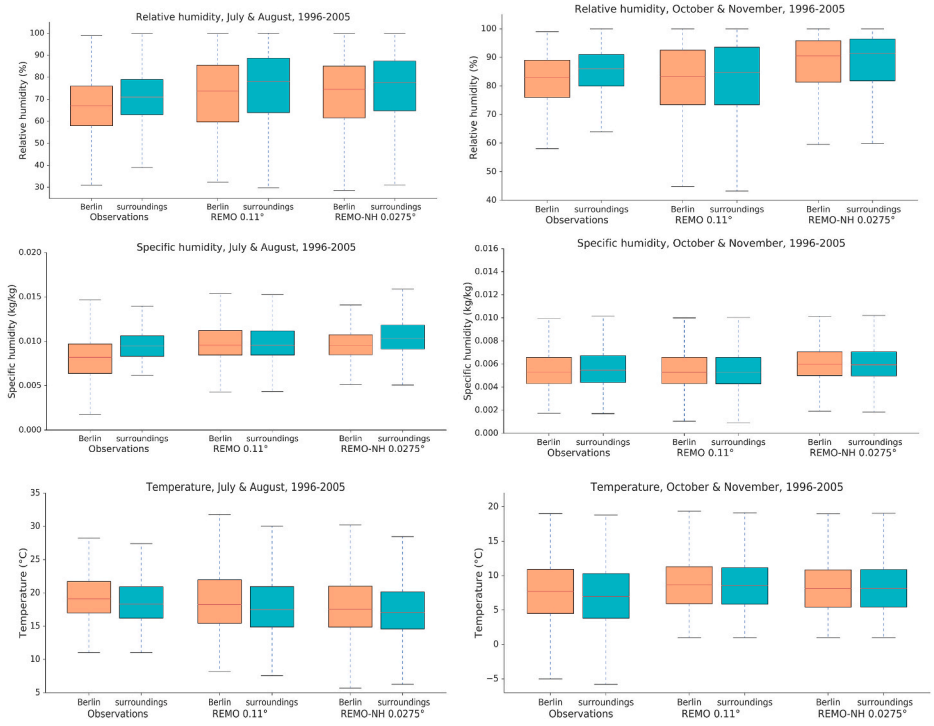

Fig. 8. Boxplots comparing observations with EUCP model output data of REMO (0.11°) and REMO-NH (0.0275°) for the variables RH, SH (no in-situ observations available through DWD), and temperature for the period 1996–2005, for the months in which the extreme conditions occur, respectively July and August (SH>0.02 kg/kg), and October and November (RH<30 %).

%. Specific humidity is lower in Berlin than its surroundings for the observations, by 0.0001 kg/kg in October–November and 0.0012 kg/kg in July–August. This urban-rural SH contrast is not well captured by the model data in October–November, but is captured in July–August on the 0.0275° horizontal resolution, showing a clear added value on the convection-permitting scale for these months. The temperature is higher by 1–2 °C in Berlin. This urban-rural contrast is largest in summer months, underpinning the SH>0.02 kg/kg extreme condition. The observations for October and November show a larger urban-rural contrast than the model simulations, for both RH (approx. −4 percentage points) and temperature (+1–2 °C). Overall, the observations are not clearly closer to the 0.11° or to the 0.0275° horizontal resolution. Concluding, when looking at these mean values no substantial added value is derived from going to finer resolutions except for the specific humidity urban-rural contrast (Fig. 8).

3.2.3. *Added value of convection-permitting simulations*

The downscaled cases, Case1 and Case2, for each extreme condition, SH>0.02 kg/kg and RH<30 %, are further analyzed to understand the differences between the spatial resolutions, for Berlin and its surroundings. Fourteen model output variables are studied for five days around the extreme condition, 2–3 days before as well as 2–3 days after the extreme peak. The 5-day time series are based on the spatial average calculated over the grid boxes representing Berlin (see black polygon Fig. 1, and Fig. 3) and its surroundings (black rectangle Fig. 1). The analysis focusses on four main aspects: 1) differences between spatial resolutions (0.11° vs. 0.0275°); 2) urban-rural contrast (Berlin vs. surroundings); 3) comparing the cases (Case1 vs. Case2 of each extreme condition); 4) comparing the extreme conditions (SH>0.02 kg/kg vs. RH<30 %).

To visually guide the analysis, Fig. 9 presents plots for eight selected key variables showing the computed differences between Berlin and its surroundings (difference = Berlin – surroundings), for the 0.11° and the 0.0275° horizontal resolution, for each case (Case1 and Case2), and for each extreme condition SH>0.02 kg/kg (Fig. 9A) and RH<30 % (Fig. 9B). The full time series, for all the fourteen model output variables are presented in the Annex (Fig. A3, Fig. A4, and Table A1).

Overall, the meteorological characteristics of the downscaled cases

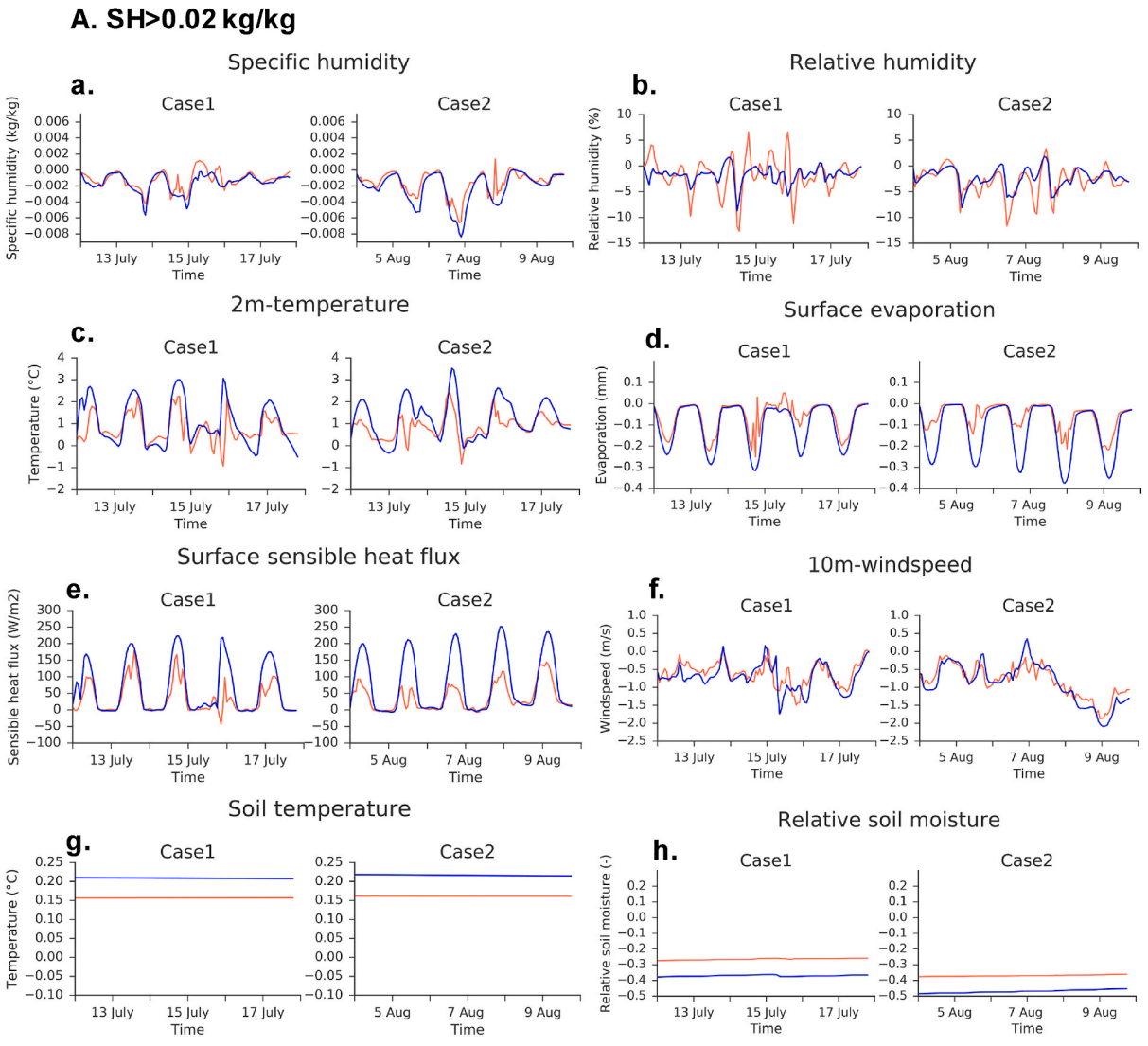

Fig. 9A. Differences plots during the 5 days around the downscaled extreme condition SH>0.02 kg/kg for each case (Case1 and Case2). Differences between Berlin and its surroundings calculated for the 0.11° and the 0.0275° resolution (difference = Berlin-surroundings).

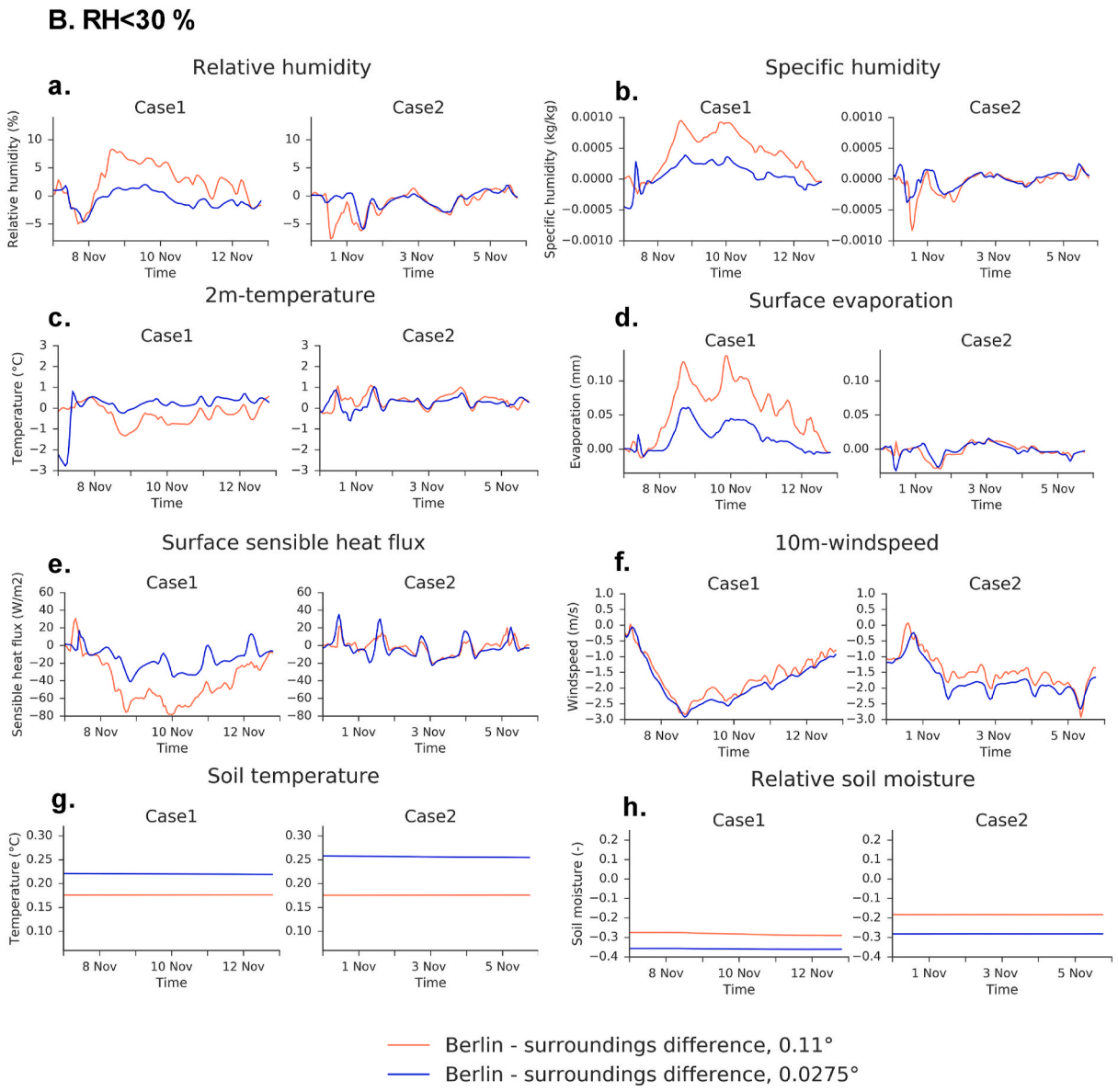

Fig. 9B. Differences plots during the 5 days around the downscaled extreme condition RH<30 % for each case (Case1 and Case2). Differences between Berlin and its surroundings calculated for the 0.11° and the 0.0275° resolution (difference = Berlin-surroundings).

are in line with the meteorological characteristics and synoptic situation described for each extreme condition on the 0.44° horizontal resolution based on the HAPPI simulations (section 3.1.2, Fig. 5, and Table 2). Among Case1 and Case2 of each of the extreme conditions, SH>0.02 kg/kg and RH<30 %, similar overall meteorological characteristics are found (Annex Fig. A3 and Fig. A4). This implies that REMO captures the extreme events and its meteorological conditions adequately in the downscaled simulations. However, detailed differences are found investigating the downscaled cases further.

Looking into the SH>0.02 kg/kg extreme condition, the two downscaled cases (CaseSH1 and CaseSH2) show that the urban area mitigates the high specific humidity levels, indicating a clear urban dry island effect, which is enhanced on the convection permitting scale (Fig. 10). On the 0.0275° horizontal resolution the SH decreases up to 0.005 kg/kg and the RH up to 20 % compared to the 0.11° horizontal resolution (Fig. 9A–a,b). Concerning the urban-rural contrast, Berlin is up to 10 % RH and up to 0.008 kg/kg SH less moist than its surroundings (Fig. 9A–a, b). Nevertheless, the city still faces high SH levels up to 0.016 kg/kg (CaseSH1) and 0.020 kg/kg (CaseSH2) on the 0.11° horizontal resolution (Fig. 10). The SH peak values are lower in Berlin for the 0.0275° horizontal resolutions, with SH levels up to 0.013 kg/kg (CaseSH1) and 0.016 kg/kg (CaseSH2) (Fig. 10). It implies extreme moist summer days will be less humid in Berlin than its surroundings under 2.0 °C global warming, particularly on the 0.0275° horizontal resolution.

The results for the RH<30 % extreme condition show, despite a small urban-rural contrast, that the downscaled extreme events will be less moist on the convection permitting scale, particularly in Berlin. On the 0.0275° horizontal resolution the SH decreases up to 0.0007 kg/kg and the RH up to 10 % compared to the 0.11° horizontal resolution (Fig. 9B–a,b). Only a small urban-rural moisture contrast is found, especially on the 0.0275° horizontal resolution. Interestingly, Berlin is moister (RH and SH) than its surroundings for the 0.11° horizontal resolution for both cases during the bottom low of the extreme condition (Fig. 10). This reverses for RH on the 0.0275° horizontal resolution, where Berlin shows lower relative humidity levels than its surroundings, particularly for CaseRH1 (Figs. 7 and 10). The small urban-rural contrast and slight urban drying effect for CaseRH1 on the 0.0275° horizontal resolution corresponds with the Boxplots (Fig. 8), which show a small urban-rural RH contrast in October and November. The findings for the RH<30 % extreme condition indicate an intensification of the dry

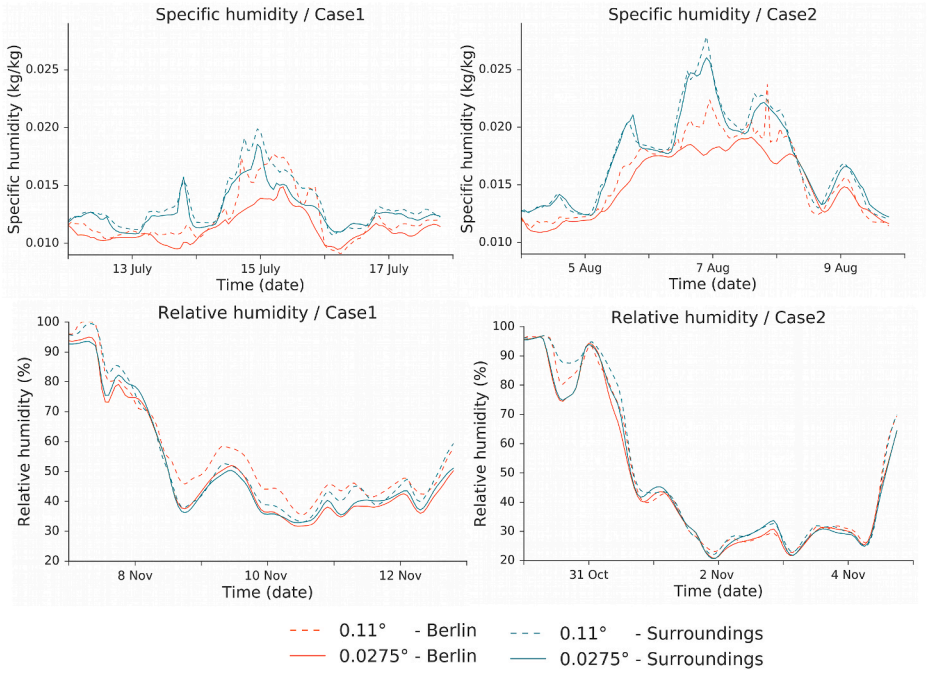

Fig. 10. 5-day time series around the extreme conditions, SH>0.02 kg/kg (top row) and RH<30 % (bottom row), for respectively SH and RH, showing Case1 and Case2, for Berlin and its surroundings, for the spatial resolutions 0.0275° and 0.11°.

extreme condition on the convection-permitting scale during the peak of the extreme events, particularly for CaseRH1.

Overall, the results for both extreme humidity conditions, SH>0.02 kg/kg and RH<30 %, show that the convection-permitting scale is less moist than the 0.11° horizontal resolution, especially in Berlin compared to its surroundings.

The intensified moisture reduction on the 0.0275° horizontal resolution in Berlin can be explained by the fact that urban areas are represented in the REMO model through a sealed "rock" surface. The urban representation is characterized by a greater heat capacity and reduced water storage, resulting in higher soil temperatures, lower soil moisture, and reduced surface evaporation, explaining the reduced humidity levels and higher temperatures in Berlin compared to its surroundings (Langendijk et al. 2019a). The model results for the respective variables show this urban effect clearly for both extreme conditions (Fig. 9A/B, Annex; Fig. A2, Fig. A3). Higher temperatures of approximately 0.5 °C–4.0 °C are found for both extreme conditions in Berlin compared to its surroundings, which is more profound by ~1.0 °C for the 0.0275° compared to 0.11° horizontal resolution (Fig. 9A/B-c). Furthermore, the soil moisture in Berlin is up to 0.3 lower than its surroundings, and the urban-rural soil moisture contrast is up to 0.1 larger on the 0.0275° than on the 0.11° horizontal resolution (Fig. 9A/B-h). In addition, the soil temperature in Berlin is up to 0.25 °C higher than its surroundings (Fig. 9A/B-g), and the urban-rural soil temperature contrast is approximately 0.05 °C larger on the 0.0275° than 0.11° horizontal resolution. The surface evaporation is up to 0.35 mm less in Berlin than its surroundings, and the urban-rural evaporation contrast is up to 0.2 mm larger on the 0.0275° compared to the 0.11° horizontal resolution (Fig. 9A/B-d).

Clearly, the typical urban characteristic are more pronounced on the 0.0275° than on the 0.11° horizontal resolution. This is mainly due to the larger amount of urban grid boxes on the 0.0275° horizontal resolution (Fig. 3). In addition, these grid boxes contain a larger urban fraction, of around 0.6–1, compared to the 0.11° horizontal resolution, with no grid boxes containing an urban fraction larger than 0.8 (Table 1). Therefore, the urban grid boxes on the convection-permitting scale are better resolved, particularly leading to a stronger reduction in moisture and stronger warming, especially in Berlin compared to its surroundings.

In summary, the presented results in this chapter show the convection-permitting scale resolves Berlin, and its typical urban characteristics, more pronounced than the 0.11° horizontal resolution. For both extreme conditions, SH>0.02 kg/kg and RH<30 %, the 0.0275° horizontal resolution is drier and warmer than the 0.11° horizontal resolution, particularly in Berlin compared to its surroundings. The convection-permitting scale mitigates the SH>0.02 kg/kg moist extreme and intensifies the RH<30 % dry extreme.

4. Discussion

This research shows how crossing spatial resolutions from ~12.5 km to ~3 km grid size affects two humidity extreme conditions, SH>0.02 kg/kg and RH<30 %, occurring under 2 °C global mean temperature change, comparing Berlin to its surroundings. The results section directly discussed the outcomes in detail, therefore this discussion section focuses on key aspects underpinning the study.

The results of this research indicate temporal mean values only show limited differences and improvements going to finer horizontal resolutions, except for the specific humidity urban-rural contrast in July–August which shows added value on the 0.0275° horizontal resolution (Fig. 8). For the extreme conditions, and its drivers, changes in the variables are clearly visible for all the downscaled cases on the finer scales, particularly for Berlin (Fig. 9). This is in line with Ban et al. (2014) and Prein et al. (2015), who indicate convection-permitting simulations show larger benefits in the tail-distributions compared to mean values.

Climate model projections are inherently subject to uncertainty. Regional climate models are dependent on global climate models for their boundary conditions, feeding in the large scale climate conditions. Global climate models may not simulate all key dynamical patterns adequately that influence natural variability and related extremes on the local scale, such as atmospheric blocking, jet stream position, or teleconnections (Sillmann et al., 2017). The HAPPI method, by its design, specifically targets to reduce the uncertainty in climate model responses

and internal variability, in order to understand the impact of an additional half degree of warming from 1.5 °C to 2.0 °C (Mitchell et al., 2017). Nevertheless, the identified extreme conditions of this research remain subject to internal variability and related uncertainties. Additionally, dynamical downscaling methods can result in model artifacts. For instance the choice of domain, spin-up, and nesting approach may result in a too strong or too weak boundary forcing, leading to misrepresenting extremes while downscaling to finer resolutions (Bellprat et al., 2019; Matte et al., 2016; Sillmann et al., 2017; von Trentini et al., 2019).

Commonly scientific studies relate their findings to observations to gain understanding about uncertainties and biases to enhance the robustness of the results. Because it is virtually impossible to compare unprecedented future extreme conditions that did not happen in the past with observations, this research took a physical process-understanding approach. The in-depth meteorological characterization of the extreme conditions validated the physical plausibility of the extremes and the underlying drivers. To further enhance the robustness of the presented results it could be desirable to assess in more detail how the spatial differences and urban-rural contrasts found in this study relate to natural and internal variability, as well as to the uncertainty arising from the downscaled model simulations. In addition, it would be beneficial to understand if slightly less extreme conditions would have similar meteorological characteristics to the downscaled extremes investigated in this research.

The results show the convection-permitting scale resolves Berlin, and its typical urban characteristics, more pronounced than the 0.11° horizontal resolution. The convection permitting scale mitigates the SH>0.02 kg/kg moist extreme and intensifies the RH<30 % dry extreme. This indicates that the convection permitting scale is able to better capture the urban characteristics than the HAPPI data (Annex; Fig. A1), as well as the 0.11° resolution. To ensure we adequately simulate climate change extremes and impacts in cities, it is important to move towards convection-permitting resolutions.

The REMO model represents urban areas through a bulk-scheme. Forgone studies show that including a sophisticated urban parameterization scheme or an urban model can enhance the urban heat island effect, improve the diurnal cycle, and potentially lead to stronger warming and increased drying in urban areas compared to the bulk-approach (Daniel et al., 2019; Karlický et al., 2018; Langendijk et al., 2019b). This implies the reduced moisture and enhanced warming found for Berlin on finer spatial resolutions in this study might get more profound using sophisticated urban schemes. It would be important for further studies to include urban parameterizations in regional climate models to adequately capture the urban effects, particularly on the convection-permitting scale (Daniel et al., 2018; Hertwig et al., 2021).

The SH>0.02 kg/kg and RH<30 % unprecedented extreme conditions may have important implications for human health. The moist extreme, SH>0.02 kg/kg, is mitigated in Berlin, particularly on the convection-permitting resolution, resulting in a reduction of moisture in the city. This implies that urban dwellers would be slightly less affected by the moist extreme than people living in the rural areas, potentially leading to a reduced mortality rate. Nevertheless, it is important to note that this unprecedented extreme moist condition happening under 2.0 °C warming would imply an overall increase in favorable conditions for heat stress compared to the historical period. The RH<30 % extreme provides favorable conditions for the spread and survival of influenza. The convection-permitting resolution shows that Berlin is drier than its surroundings, potentially leading to increased influenza in the city with negative effects on the health of urban dwellers.

This research focuses solely on two humidity extreme conditions in Berlin and its surroundings. It would be important to understand the changes and benefits on the convection-permitting resolution for different types of extremes and for other cities. Further studies on climate extremes in urban areas, with additional regional climate models that potentially include sophisticated urban schemes, could be beneficial to compare the results of this study.

5. Summary and conclusions

This research investigates how crossing spatial resolutions from ~12.5 km to ~3 km grid size affects humidity extremes and related variables under 2 °C global mean temperature change for Berlin and its surroundings. Two meteorologically plausible unprecedented categories of future extreme humidity conditions are identified for Berlin and its surroundings based on statistical distributions of the HAPPI data, respectively SH>0.02 kg/kg and RH<30 %. Two example cases of each extreme condition are downscaled following a double-nesting approach, from the 0.44° to the 0.11° horizontal resolution by REMO and thereafter from the 0.11° to the 0.0275° horizontal resolution with REMO-NH. The differences between the spatial resolutions and the urban-rural contrast are analyzed for Berlin and its surroundings, following a meteorological process-understanding approach.

The main results show that the convection-permitting scale resolves Berlin, and its typical urban characteristics, more pronounced than the 0.11° horizontal resolution. The 0.0275° horizontal resolution is less moist than the 0.11° horizontal resolution for the downscaled cases of both extreme conditions, for SH>0.02 kg/kg (0.005 kg/kg SH and 20 % RH) and for RH<30 % (0.0007 kg/kg SH and 10 % RH). Higher temperatures of approximately 1.0 °C–2.0 °C are found for both extreme conditions for the 0.0275° simulations compared to 0.11° horizontal resolution. The differences between the 0.11° to the 0.0275° horizontal resolution are generally more profound in Berlin compared to its surroundings, especially indicating warmer temperatures and a stronger decrease in moisture (RH and SH) on the 0.0275° horizontal resolution in the city. This urban drying effect and the associated urban-rural contrast is larger for the SH>0.02 kg/kg extreme condition compared to the RH<30 % extreme condition, particularly on the convection-permitting scale. The convection-permitting scale mitigates the SH>0.02 kg/kg moist extreme and intensifies the RH<30 % dry extreme.

The enhanced reduction in moisture is predominantly due to the increase of urban grid boxes with larger urban fractions on the 0.0275° horizontal resolution compared to the 0.11° horizontal resolution. On the 0.0275° horizontal resolution the underpinning variables show higher 2-m temperatures, higher soil temperatures, lower soil moisture, reduced surface evaporation, and lower wind speeds, especially in Berlin. This implies the sealed urban surface is resolved more profoundly on the 0.0275° horizontal resolution. It demonstrates the improved capability of the convection-permitting simulations to capture the typical urban drying effect in Berlin for the two extreme conditions.

The results for the SH>0.02 kg/kg extreme condition imply that extreme moist summer days will be less humid in Berlin than its surroundings under 2.0 °C global warming, particularly when simulated on the convection-permitting scale. This humidity reduction could partly mitigate human heat stress in the city during the extreme event compared to its surroundings, potentially reducing the mortality rate. The RH<30 % extreme condition, with its low relative humidity values, could possibly favor the spread and survival of influenza particularly in Berlin, leading to negative health effects. Follow-up studies would be needed to further investigate the relationships between the extremes and various sectors, and applications. This could inform the development of climate information and services for urban areas, as well as the modelling needs and directions for RCM developments in the context of cities.

Declaration of competing interest

The authors declare that they have no known competing financial interests or personal relationships that could have appeared to influence the work reported in this paper.

Acknowledgements

We thank the "Half a degree Additional warming, Prognosis and Projected Impacts (HAPPI)" project (https://www.happimip.org/) for making the data available which enabled this research. We would like to express great gratitude to the GERICS staff members working on REMO development for their support while conducting the REMO simulations, and particularly thank them for their help to fix technical model errors; Lars Buntemeyer, Thomas Frisius, Joni-Pekka Pietikäinen, and Thomas Remke. We are grateful for the helpful suggestions by our colleague Joni-Pekka Pietikäinen to improve the first draft of the manuscript. We would like to thank the staff members at the German Climate Computing Center (DKRZ) for their technical expertise and support. The research was kindly funded by the Climate Service Center Germany (GERICS), Helmholtz-Zentrum Hereon, Germany.

Appendix A. Supplementary data

Supplementary data related to this article can be found at https://doi.org/10.1016/j.wace.2021.100367.

Author contributions

Conceptualization; G.S.L., D.R., K.S., D.J. Data curation; G.S.L. Formal analysis; G.S.L. Investigation; G.S.L. Methodology; G.S.L. Supervision; D.R., K.S., D.J. Validation; G.S.L. Visualization; G.S.L. Writing – original draft; G.S.L. Writing - review & editing; G.S.L., D.R., K.S., D.J.

References

Aerts, J., Botzen, W., 2014. Adaptation: cities' response to climate risks. Nat. Clim. Change 4, 759–760. https://doi.org/10.1038/nclimate2343.

Alexander, L.V., 2016. Global observed long-term changes in temperature and precipitation extremes: a review of progress and limitations in IPCC assessments and beyond. Weather Clim. Extrem. 11, 4–16. https://doi.org/10.1016/j.wace.2015.10.007.

Amt für Statistik Berlin-Brandenburg, 2020. Statistiken Berlin und Brandenburg [WWW Document]. Statistiken. URL. https://www.statistik-berlin-brandenburg.de/statistiken/Inhalt-Statistiken.asp. accessed 7.26.19.

Argüeso, D., Di Luca, A., Evans, J.P., 2016. Precipitation over urban areas in the western Maritime Continent using a convection-permitting model. Clim. Dynam. 47, 1143–1159. https://doi.org/10.1007/s00382-015-2893-6.

Bai, X., Dawson, R.J., Ürge-Vorsatz, D., Delgado, G.C., Salisu Barau, A., Dhakal, S., Dodman, D., Leonardsen, L., Masson-Delmotte, V., Roberts, D.C., Schultz, S., 2018. Six research priorities for cities and climate change. Nature 23–25. https://doi.org/10.1038/d41586-018-02409-z.

Baklanov, A., Grimmond, C.S.B., Carlson, D., Terblanche, D., Tang, X., Bouchet, V., Lee, B., Langendijk, G., Kolli, R.K., Hovsepyan, A., 2018. From urban meteorology, climate and environment research to integrated city services. Urban Clim 23, 330–341. https://doi.org/10.1016/j.uclim.2017.05.004.

Ban, N., Schmidli, J., Schär, C., 2014. Evaluation of the convection-resolving regional climate modeling approach in decade-long simulations. J. Geophys. Res. 119, 7889–7907. https://doi.org/10.1002/2014JD021478.

Bellprat, O., Guemas, V., Doblas-reyes, F., Donat, M.G., 2019. Event attribution. Nat. Commun. 10, 29–31. https://doi.org/10.1038/s41467-019-09729-2.

Coccolo, S., Kämpf, J., Scartezzini, J.L., Pearlmutter, D., 2016. Outdoor Human Comfort and Thermal Stress: A Comprehensive Review on Models and Standards. Urban Clim. https://doi.org/10.1016/j.uclim.2016.08.004.

Coppola, E., Sobolowski, S., Pichelli, E., Raffaele, F., Ahrens, B., Anders, I., Ban, N., Bastin, S., Belda, M., Belusic, D., Caldas-Alvarez, A., Cardoso, R.M., Davolio, S., Dobler, A., Fernandez, J., Fita, L., Fumiere, Q., Giorgi, F., Goergen, K., Güttler, I., Halenka, T., Heinzeller, D., Hodnebrog, Jacob, D., Kartsios, S., Katragkou, E., Kendon, E., Khodayar, S., Kunstmann, H., Knist, S., Lavín-Gullón, A., Lind, P., Lorenz, T., Maraun, D., Marelle, L., van Meijgaard, E., Milovac, J., Myhre, G., Panitz, H.J., Piazza, M., Raffa, M., Raub, T., Rockel, B., Schär, C., Sieck, K., Soares, P.M.M., Somot, S., Srnec, L., Stocchi, P., Tölle, M.H., Truhetz, H., Vautard, R., de Vries, H., Warrach-Sagi, K., 2020. A first-of-its-kind multi-model convection permitting ensemble for investigating convective phenomena over Europe and the Mediterranean. Clim. Dynam. 55, 3–34. https://doi.org/10.1007/s00382-018-4521-8.

Dalziel, B.D., Kissler, S., Gog, J.R., Viboud, C., Bjørnstad, O.N., Metcalf, C.J.E., Grenfell, B.T., 2018. Urbanization and humidity shape the intensity of influenza epidemics in U.S. cities. Science (80- 362, 75–79. https://doi.org/10.1126/science.aat6030.

Daniel, M., Lemonsu, A., Déqué, M., Somot, S., Alias, A., Masson, V., 2019. Benefits of explicit urban parameterization in regional climate modeling to study climate and city interactions. Clim. Dynam. 5, 2745–2764. https://doi.org/10.1007/s00382-018-4289-x.

Daniel, M., Lemonsu, A., Déqué, M., Somot, S., Alias, A., Masson, V., 2018. Benefits of explicit urban parameterization in regional climate modeling to study climate and city interactions. Clim. Dynam. 1–20. https://doi.org/10.1007/s00382-018-4289-x.

Davis, R.E., McGregor, G.R., Enfield, K.B., 2016. Humidity: a review and primer on atmospheric moisture and human health. Environ. Res. 144, 106–116. https://doi.org/10.1016/j.envres.2015.10.014.

Denis, B., Laprise, R., Caya, D., Côté, J., 2002. Downscaling ability of one-way nested regional climate models: the Big-Brother Experiment. Clim. Dynam. 18, 627–646. https://doi.org/10.1007/s00382-001-0201-0.

Dwd, D., 2021. German weather service, climate data center (CDC) [WWW Document]. URL. https://cdc.dwd.de/portal/. accessed 5.8.21.

Dwd, D.W.D., 2019. German weather service, climate data center (CDC) [WWW Document]. URL. https://cdc.dwd.de/portal/. accessed 1.25.19.

EEA, 2000. The revised and supplemented Corine land cover nomenclature. EEA Tech. Rep 40.

Fischer, E.M., Knutti, R., 2013. Robust projections of combined humidity and temperature extremes. Nat. Clim. Change 3, 126–130. https://doi.org/10.1038/nclimate1682.

Gates, W.L., 1992. AMIP: the atmospheric model Intercomparison project. Bull. Am. Meteorol. Soc. 73, 1962–1970. https://doi.org/10.1175/1520-0477(1992)073<1962:ATAMIP>2.0.CO;2.

Goettel, H., 2009. Einfluss der nichthydrostatischen Modellierung und der Niederschlagsverdriftung auf die Ergebnisse regionaler Klimamodellierung. Reports Earth Syst. Sci. 125.

Grimmond, C.S.B., Roth, M., Oke, T.R., Au, Y.C., Best, M., Betts, R., Carmichael, G., Cleugh, H., Dabberdt, W., Emmanuel, R., Freitas, E., Fortuniak, K., Hanna, S., Klein, P., Kalkstein, L.S., Liu, C.H., Nickson, A., Pearlmutter, D., Sailor, D., Voogt, J., 2010. Climate and more sustainable cities: climate information for improved planning and management of cities (Producers/Capabilities Perspective). In: Procedia Environmental Sciences. https://doi.org/10.1016/j.proenv.2010.09.016.

Hage, K.D., 1975. Urban-rural humidity differences. J. Appl. Meteorol. 7, 1277–1283. https://doi.org/10.1175/1520-0450(1975)014<1277:urhd>2.0.co;2.

Hardwick Jones, R., Westra, S., Sharma, A., 2010. Observed relationships between extreme sub-daily precipitation, surface temperature, and relative humidity. Geophys. Res. Lett. 37 https://doi.org/10.1029/2010GL045081.

Herceg, D., Sobel, A.H., Liqiang, S., Zebiak, S.E., 2006. The Big Brother Experiment and seasonal predictability in the NCEP regional spectral model. Clim. Dynam. 27, 69–82. https://doi.org/10.1007/s00382-006-0130-z.

Hertwig, D., Ng, M., Grimmond, S., Vidale, P.L., McGuire, P.C., 2021. High-resolution global climate simulations: representation of cities. Int. J. Climatol. 5, 3266–3285. https://doi.org/10.1002/joc.7018.

IPCC, 2012. In: Field, C.B., Barros, V., Stock, T.F., Qin, D., Dokken, D.J., Ebi, K.L., Mastrandrea, M.D., Mach, K.J., Plattner, G.-K., Allen, S.K., Tignor, M., Midgley, P.M. (Eds.), Managing the Risks of Extreme Events and Disasters to Advance Climate Change Adaptation: Special Report of the Intergovernmental Panel on Climate Change. A Spec. Rep. Work. Groups I II Intergov. Panel Clim. Chang., vol. 9781107025, pp. 1–582. https://doi.org/10.1017/CBO9781139177245.

Jacob, D., Elizalde, A., Haensler, A., Hagemann, S., Kumar, P., Podzun, R., Rechid, D., Remedio, A.R., Saeed, F., Sieck, K., Teichmann, C., Wilhelm, C., 2012a. Assessing the transferability of the regional climate model REMO to different coordinated regional climate downscaling experiment (CORDEX) regions. Atmosphere 3, 181–199. https://doi.org/10.3390/atmos3010181.

Jacob, D., Haensler, A., Saeed, F., Elizalde, A., Hagemann, S., Kumar, P., Podzun, R., Rechid, D., Remedio, A.R., Sieck, K., Teichmann, C., Wilhelm, C., 2012b. Assessing the transferability of the regional climate model REMO to different coordinated regional climate downscaling experiment (CORDEX) regions. Atmosphere 3 (1), 181–199. https://doi.org/10.3390/atmos3010181.

Jacob, D., Podzun, R., 1997. Sensitivity studies with the regional climate model REMO. Meteorol. Atmos. Phys. 63 (1), 119–129. https://doi.org/10.1007/BF01025368.

Jacob, D., Teichmann, C., Sobolowski, S., Katragkou, E., Anders, I., Belda, M., Benestad, R., Boberg, F., Buonomo, E., Cardoso, R.M., Casanueva, A., Christensen, O.B., Christensen, J.H., Coppola, E., De Cruz, L., Davin, E.L., Dobler, A., Domínguez, M., Fealy, R., Fernandez, J., Gaertner, M.A., García-Díez, M., Giorgi, F., Gobiet, A., Goergen, K., Gómez-Navarro, J.J., Alemán, J.J.G., Gutiérrez, C., Gutiérrez, J.M., Güttler, I., Haensler, A., Halenka, T., Jerez, S., Jiménez-Guerrero, P., Jones, R.G., Keuler, K., Kjellström, E., Knist, S., Kotlarski, S., Maraun, D., van Meijgaard, E., Mercogliano, P., Montávez, J.P., Navarra, A., Nikulin, G., de Noblet-Ducoudré, N., Panitz, H.J., Pfeifer, S., Piazza, M., Pichelli, E., Pietikäinen, J.P., Prein, A.F., Preuschmann, S., Rechid, D., Rockel, B., Romera, R., Sánchez, E., Sieck, K., Soares, P.M.M., Somot, S., Srnec, L., Sørland, S.L., Termonia, P., Truhetz, H., Vautard, R., Warrach-Sagi, K., Wulfmeyer, V., 2020. Regional climate downscaling over Europe: perspectives from the EURO-CORDEX community. Reg. Environ. Change 20. https://doi.org/10.1007/s10113-020-01606-9.

Jerez, S., López-Romero, J.M., Turco, M., Lorente-Plazas, R., Gómez-Navarro, J.J., Jiménez-Guerrero, P., Montávez, J.P., 2020. On the spin-up period in WRF simulations over Europe: trade-offs between length and seasonality. J. Adv. Model. Earth Syst. 12, 1–18. https://doi.org/10.1029/2019MS001945.

Karlický, J., Huszár, P., Halenka, T., Belda, M., Žák, M., Pišoft, P., Mikšovský, J., 2018. Multi-model comparison of urban heat island modelling approaches. Atmos. Chem. Phys. 18, 10655–10674. https://doi.org/10.5194/acp-18-10655-2018.

Kotlarski, S., Keuler, K., Christensen, O.B., Colette, A., Déqué, M., Gobiet, A., Goergen, K., Jacob, D., Lüthi, D., Van Meijgaard, E., Nikulin, G., Schär, C., Teichmann, C., Vautard, R., Warrach-Sagi, K., Wulfmeyer, V., 2014. Regional climate modeling on European scales: a joint standard evaluation of the EURO-

CORDEX RCM ensemble. Geosci. Model Dev. (GMD) 7, 1297–1333. https://doi.org/10.5194/gmd-7-1297-2014.

Langendijk, G.S., Aubry-Wake, C., Osman, M., Gulizia, C., Attig-Bahar, F., Behrens, E., Bertoncini, A., Hart, N., Indasi, V.S., Innocenti, S., van der Linden, E.C., Mamnun, N., Rasouli, K., Reed, K.A., Ridder, N., Rivera, J., Ruscica, R., Ukazu, B.U., Walawender, J.P., Walker, D.P., Woodhams, B.J., Yilmaz, Y.A., 2019a. Three ways forward to improve regional information for extreme events: an early career perspective. Front. Environ. Sci. 7 https://doi.org/10.3389/fenvs.2019.00006.

Langendijk, G.S., Rechid, D., Jacob, D., 2019b. Urban areas and urban-rural contrasts under climate change: what does the EURO-CORDEX ensemble tell us?-Investigating near surface humidity in berlin and its surroundings. Atmosphere 10. https://doi.org/10.3390/ATMOS10120730.

Leps, N., Brauch, J., Ahrens, B., 2019. Sensitivity of limited area atmospheric simulations to lateral boundary conditions in idealized experiments. J. Adv. Model. Earth Syst. 11, 2694–2707. https://doi.org/10.1029/2019MS001625.

Li, D., Yuan, J., Kopp, R.E., 2020. Escalating global exposure to compound heat-humidity extremes with warming. Environ. Res. Lett. 6 (064003) https://doi.org/10.1088/1748-9326/ab7d04.

Lokoshchenko, M.A., 2017. Urban heat island and urban dry island in Moscow and their centennial changes. J. Appl. Meteorol. Climatol. 10, 2729–2745. https://doi.org/10.1175/JAMC-D-16-0383.1.

Lowe, J.A., McSweeney, C., Hewitt, C., 2020. An overview of the EUCP project-towards improved European Climate Predictions and Projections. EGU Gen. Assem. Conf. Abstr. 19475.

Lowen, A.C., Mubareka, S., Steel, J., Palese, P., 2007. Influenza virus transmission is dependent on relative humidity and temperature. PLoS Pathog. 3, 1470–1476. https://doi.org/10.1371/journal.ppat.0030151.

Majewski, D., 1991. The europa-modell of the deutscher wetterdienst. ECMWF Semin. Numer. methods Atmos. Model. 2, 147–191.

Masson, V., Lemonsu, A., Hidalgo, J., Voogt, J., 2020. Urban climates and climate change. Annu. Rev. Environ. Resour. 45, 411–444. https://doi.org/10.1146/annurev-environ-012320-083623.

Matte, D., Laprise, R., Thériault, J.M., 2016. Comparison between high-resolution climate simulations using single- and double-nesting approaches within the Big-Brother experimental protocol. Clim. Dynam. 47, 3613–3626. https://doi.org/10.1007/s00382-016-3031-9.

Matte, D., Laprise, R., Thériault, J.M., Lucas-Picher, P., 2017. Spatial spin-up of fine scales in a regional climate model simulation driven by low-resolution boundary conditions. Clim. Dynam. 49, 563–574. https://doi.org/10.1007/s00382-016-3358-2.

Mishra, V., Ganguly, A.R., Nijssen, B., Lettenmaier, D.P., 2015. Changes in observed climate extremes in global urban areas. Environ. Res. Lett. 10, 024005 https://doi.org/10.1088/1748-9326/10/2/024005.

Mitchell, D., AchutaRao, K., Allen, M., Bethke, I., Beyerle, U., Ciavarella, A., Forster, P. M., Fuglestvedt, J., Gillett, N., Haustein, K., Ingram, W., Iversen, T., Kharin, V., Klingaman, N., Massey, N., Fischer, E., Schleussner, C.-F., Scinocca, J., Seland, Ø., Shiogama, H., Shuckburgh, E., Sparrow, S., Stone, D., Uhe, P., Wallom, D., Wehner, M., Zaaboul, R., 2017. Half a degree additional warming, prognosis and projected impacts (HAPPI): background and experimental design. Geosci. Model Dev. (GMD) 10, 571–583. https://doi.org/10.5194/gmd-10-571-2017.

Myhre, G., Alterskjær, K., Stjern, C.W., Hodnebrog, Marelle, L., Samset, B.H., Sillmann, J., Schaller, N., Fischer, E., Schulz, M., Stohl, A., 2019. Frequency of extreme precipitation increases extensively with event rareness under global warming. Sci. Rep. 9 (1), 1–10. https://doi.org/10.1038/s41598-019-52277-4.

Pietikäinen, J.P., O'Donnell, D., Teichmann, C., Karstens, U., Pfeifer, S., Kazil, J., Podzun, R., Fiedler, S., Kokkola, H., Birmili, W., O'Dowd, C., Baltensperger, U., Weingartner, E., Gehrig, R., Spindler, G., Kulmala, M., Feichter, J., Jacob, D., Laaksonen, A., 2012. The regional aerosol-climate model REMO-HAM. Geosci. Model Dev. (GMD) 5, 1323–1339. https://doi.org/10.5194/gmd-5-1323-2012.

Prein, A.F., Langhans, W., Fosser, G., Ferrone, A., Ban, N., Goergen, K., Keller, M., Tölle, M., Gutjahr, O., Feser, F., Brisson, E., Kollet, S., Schmidli, J., Van Lipzig, N.P. M., Leung, R., 2015. A review on regional convection-permitting climate modeling: demonstrations, prospects, and challenges. Rev. Geophys. 53, 323–361. https://doi.org/10.1002/2014RG000475.

Raymond, C., Matthews, T., Horton, R.M., 2020. The emergence of heat and humidity too severe for human tolerance. Sci. Adv. 6 https://doi.org/10.1126/sciadv.aaw1838.

Rechid, D., Jacob, D., 2006. Influence of monthly varying vegetation on the simulated climate in Europe. Meteorol. Z. 15, 99–116. https://doi.org/10.1127/0941-2948/2006/0091.

Roeckner, E., Arpe, K., Bengtsson, L., Christoph, M., Claussen, M., Dümenil, L., Esch, M., Giorgetta, M., Schlese, U., Schulzweida, U., 1996. The atmospheric general circulation model ECHAM-4: model description and simulation of present-day climate. MPI Rep 218, 171.

Rosenzweig, C., Solecki, W., Romero-Lankao, P., Mehrotra, S., Dhakal, S., Bowman, T., Ibrahim, S.A., 2018. Climate change and cities: second assessment report of the urban climate change research network. In: Climate Change and Cities. https://doi.org/10.1017/9781316563878.007.

Semmler, T., 2002. Der Wasser- und Energiehaushalt der arktischen Atmosphäre. Examensarbeit - Max-Planck-Institut fur Meteorol, pp. 101–106.

Shaman, J., Kohn, M., 2009. Absolute humidity modulates influenza survival, transmission, and seasonality. Proc. Natl. Acad. Sci. Unit. States Am. 106, 3243–3248. https://doi.org/10.1073/PNAS.0806852106.

Shaman, J., Pitzer, V.E., Viboud, C., Grenfell, B.T., Lipsitch, M., 2010. Absolute humidity and the seasonal onset of influenza in the continental United States. PLoS Biol. 8 https://doi.org/10.1371/journal.pbio.1000316.

Sharma, A.S., Baker, D.N., Bhattacharyya, A., Bunde, A., Dimri, V.P., Gupta, H.K., Gupta, V.K., Lovejoy, S., Main, I.G., Schertzer, D., Von Storch, H., Watkins, N.W., 2013. Complexity and extreme events in geosciences: an overview. Extrem. Events Nat. Hazards Complex. Perspect 1–16. https://doi.org/10.1029/2012GM001233.

Sieck, K., Nam, C., Bouwer, L.M., Rechid, D., Jacob, D., 2021. Weather Extremes over Europe under Regional Climate Ensemble Simulations, pp. 457–468.

Sillmann, J., Thorarinsdottir, T., Keenlyside, N., Schaller, N., Alexander, L.V., Hegerl, G., Seneviratne, S.I., Vautard, R., Zhang, X., Zwiers, F.W., 2017. Understanding, modeling and predicting weather and climate extremes: challenges and opportunities. Weather Clim. Extrem. 18, 65–74. https://doi.org/10.1016/j.wace.2017.10.003.

Spänkuch, D., Güldner, J., Steinhagen, H., Bender, M., 2011. Analysis of a dryline-like feature in northern Germany detected by ground-based microwave profiling. Meteorol. Z. 20, 409–421. https://doi.org/10.1127/0941-2948/2011/0222.

Stevens, B., Giorgetta, M., Esch, M., Mauritsen, T., Crueger, T., Rast, S., Salzmann, M., Schmidt, H., Bader, J., Block, K., Brokopf, R., Fast, I., Kinne, S., Kornblueh, L., Lohmann, U., Pincus, R., Reichler, T., Roeckner, E., 2013. Atmospheric component of the MPI-M earth system model: ECHAM6. J. Adv. Model. Earth Syst. 5, 146–172. https://doi.org/10.1002/jame.20015.

Stull, R., 2017. Practical Meteorology: an Algebra-Based Survey of Atmospheric Science. Univ. of British Columbia.

von Trentini, F., Leduc, M., Ludwig, R., 2019. Assessing natural variability in RCM signals: comparison of a multi model EURO-CORDEX ensemble with a 50-member single model large ensemble. Clim. Dynam. 53, 1963–1979. https://doi.org/10.1007/s00382-019-04755-8.

Wiesner, S., Bechtel, B., Fischereit, J., Gruetzun, V., Hoffmann, P., Leitl, B., Rechid, D., Schlünzen, K., Thomsen, S., 2018. Is it possible to distinguish global and regional climate change from urban land cover induced signals? A mid-latitude city example. Urban Sci 2, 12. https://doi.org/10.3390/urbansci2010012.